Detection of Faint GEO Objects Using Population and Motion Prediction

Masahiko Uetsuhara, Toshiya Hanada, Hitoshi Yamaoka, Tomoko Fujiwara
Kyushu University
Toshifumi Yanagisawa, Hirohisa Kurosaki
Japan Space Exploration Agency
Yukihito Kitazawa
IHI Corporation

ABSTRACT

This paper proposes to apply orbital debris modeling techniques, which describes debris generation and propagation to define debris environment, to ground-based optical measurements that may be most effective in space situational awareness in GEO. The techniques enable us to predict population of debris from confirmed and/or unconfirmed breakup events. The predicted debris population specifies effectively when, where and how we should conduct optical measurements using ground-based telescopes. The techniques also enable us to predict motion of debris. The predicted debris motion specifies effectively and precisely how we should process image sequences of objects in GEO, acquired using ground-based telescopes. This paper also applies the proposed approach to small telescopes with 1 m and smaller aperture and to hypothetical breakup events in and near GEO to demonstrate. Results from actual measurements performed conclude that the proposed approach can conduct predictive analyses of space objects that include characterizing, tracking and predicting the behavior of individual and groups of space objects and conduct image processing methods to effectively decrease limitation on remote imaging of space objects.

1. INTRODUCTION

GEO is the unique and valuable region where hundreds of infrastructures such as communications, weather and data-relay satellites are in operation. To date, the Space Surveillance Network (SSN) cataloged one thousand or more objects, down to approximately 1 m in size, in GEO [1]. Other observations performed by the European Space Agency (ESA) using the Tenerife telescope have indicated that the GEO population, to a limiting diameter of approximately 10 cm, exceeds the cataloged population by a factor of four [2]. However, only 400 objects or less in GEO are controlled inside their longitude slot to be considered as operational [3]. Those operational satellites are under threat of collisions with unknown objects (a.k.a. debris). Therefore, measurements of unknown objects are necessary to accurately define debris environment in GEO and to conduct reliable risk assessments for those operational satellites. One of major tasks for revealing the population of unknown objects can breakdown into developing faster and more precise algorithm to detect faint objects (e.g. 1 meter and smaller objects in GEO or much lower than 17th magnitude brightness objects). Optical observation is a well-known method of orbit determination and space situational awareness for deep space (e.g. GEO) objects [4, 5]. Our objective is to detect faint GEO debris by small telescopes that exist enough around the world to reveal the GEO populations.

Detection methods for moving celestial objects can be two folds: 1) Detect-Before-Track (DBT), and 2) Track-Before-Detect (TBD) [6]. DBT methods detect features in each spatial-temporal image first, and then track individual features to estimate their trajectory. The signal-to-noise ratio (S/N) detectable with DBT methods is reasonably high so as individual features are recognizable by naked eyes. On the other hand, TBD methods assume appropriate hypothetical trajectories in a sequence of spatial-temporal images first, and then stack each image by shifting along the hypothesized trajectories to emphasize moving dark objects. Therefore, the S/N detectable with TBD is relatively low in comparison to DBT, and can reach down to 1 theoretically and ideally. Since large telescopes can observe faint debris with sufficient S/N a combination of large telescopes and DBT methods have been believed as the most effective solution. A combination of small telescopes and TBD methods also could be an effective solution to detect faint debris. As illustrated in Fig. 1, TBD methods can detect darker objects, compared to performance of the telescopes. A problem here is that TBD methods may require longer computational time to detect moving dark objects. However, computational time can be reduced effectively and drastically if appropriate hypothetical trajectories are provided. Orbital debris modeling (ODM) techniques, which describe debris generation and propagation to define debris environment, enable us to predict motion of debris. The predicted debris motion

specifies effectively and precisely how we should process image sequences of objects in GEO, acquired using ground-based telescopes. Therefore, this paper proposed to apply the ODM techniques to TBD methods.

This paper also proposes to apply the ODM techniques to specify effectively when, where, and how we should conduct optical measurements using ground-based telescopes. Current debris search strategies for ground-based telescopes observing in GEO are designed around the known orbital distributions of cataloged objects. However, the majority of cataloged objects are believed to be intact spacecraft and rocket bodies, not the debris particles the searches are intended to locate. If there have been breakup events in GEO, the explosions may have put the debris into orbits that are significantly different from those in the catalog. Consequently, observation plans optimized for the catalog population may not be optimized for any unseen debris populations. This paper optimizes observation plans for debris particles from unconfirmed breakup events in GEO, published in literatures, to search and feature them. The ODM techniques enable us to conduct predictive analyses of space objects that include characterizing, tracking and predicting the behavior of individual and groups of space objects, and to proceed image processing methods to effectively decrease limitation on remote imaging of space objects.

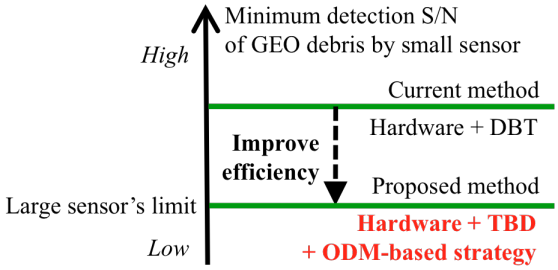

Fig. 1. Targeting performance of proposed method

2. STRATEGY AND APPROACH

Fig. 2(a) schematically describes the "ODM-based strategy," starting with information on confirmed and/or unconfirmed breakup events. Procedures, which this paper proposes to apply the ODM techniques to, include: 1) "planning and observation," and 2) "processing and detection." Both procedures will be based upon the outcome of ODM techniques (i.e. predicted population and motion). The strategy also includes another procedure entitled "origin identification."

2.1 Population and Motion Prediction

ODM techniques to be applied for population and motion prediction are debris generation and propagation. Both predictions are performed by a common flow as illustrated in Fig. 2(b). First, debris fragments down to 10 cm in size are generated from confirmed and/or unconfirmed breakup events in GEO using the NASA standard breakup model 2001 revision described in [7]. Debris generation has significant uncertainty in nature so that it is unfeasible or impossible to compute an exact result with a deterministic algorithm. Therefore, a Monte Carlo (MC) method is applied to aggregate the results of the individual computations into the final result. Preliminary analysis conducted for this study indicates that 60 iterations or more are needed to get a statistically averaged result. Second, debris orbits are propagated till planned observation epoch and generate "snapshots" at a proper time interval during planned observation period. Each snapshot contains orbital elements of all debris at a given time. Orbit perturbations to be considered for the propagation are non-spherical part of the Earth gravity, solar radiation pressure effects, and gravitational attractions due to the Sun and Moon.

The geocentric equatorial coordinates (i.e. right ascension (RA) and declination (Dec)) of all debris are calculated using the snapshots to predict the probability that the generated debris will be in each bin defined by the geocentric equatorial coordinates. All snapshots that each MC run generates for a given time are merged into one population prediction to specify effectively when, where and how we should conduct optical measurements. Dimension of each bin can be set equally to the field-of-view of selected ground-based telescope's charge-coupled device (CCD) sensor. As just described, a "spherical forecast" can be provided as the outcome of population prediction for planning and observation.

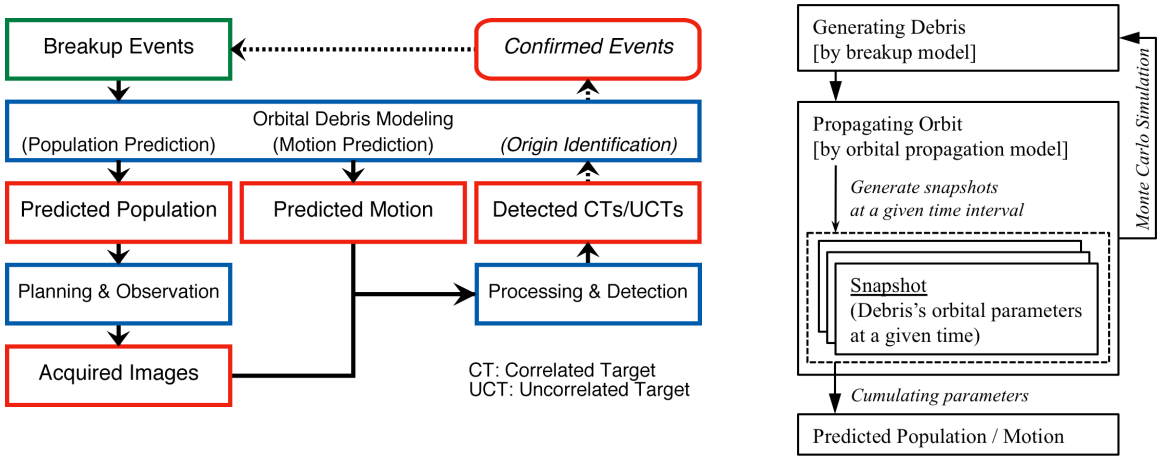

(a) ODM-based strategy overview

(b) Detailed approach among population and motion prediction

Fig. 2. ODM-based strategy

Two-dimensional shift values $\mathbf{p} = (\Delta x, \Delta y)$ in a set of image sequences of a planned observation region are also calculated using the snapshots to generate the **p** distribution that provides the probability of two-dimensional shift values of each fragment will be in each bin defined by pixels. Usually, GEO objects seem to move linearly in a set of spatial temporal images so that the two-dimensional shift values **p** can be assumed to be linear. All snapshots that each MC run generates for a given time are merged into one **p** distribution prediction to specify effectively and precisely how we should process image sequences of objects in GEO, acquired using ground-based telescopes. Thus, a "**p** distribution" can be provided as the outcome of motion prediction for processing and detection. It may be noted that the "**p** distribution" also specifies how we should conduct optical measurements.

2.2 Planning and Observation

Observations are planned and performed referring to the spherical forecasts in the previous sub-section to acquire spatial-temporal images. Here we select observation regions indicating higher probability density in the spherical forecast, considering the tracking method of telescope and the avoidances of right pollution by other bright stars and blind directions by surrounding environments at a planned observation site.

2.3 Processing & Detection

Debris will be detected in acquired spatial-temporal images by DBT and/or TBD methods. If once detected debris is correlated with the catalog, the debris is labeled as correlated target (CT). Otherwise labeled as uncorrelated target (UCT). In case of using TBD method, **p** distribution is utilized to define a superimposing vector of spatial-temporal images.

2.4 Origin Identification

The origin of each UCT will be identified at the procedure of origin identification. Details of the origin identification procedure are to be determined. As in the population and motion prediction, we also apply the ODM techniques to this procedure. Or, as will be mentioned later, the **p** distribution may assist this procedure. If once we identify origin and/or breakup event that released UCTs, we can catalog UCTs and conduct modeling in detail the confirmed breakup events. Then, we can also conduct another measurement with feedback from each measurement.

3. POPULATION AND MOTION PREDICTION

This paper simulates 25 suspected breakup events cited in literatures [8-10] and calculates the spherical forecast and **p** distribution derived from each breakup event. The following sub-sections describe the suspected breakup events, simulation conditions and results and remarks from the simulations.

3.1 Suspected Breakup Events

As specified in Table 1, so many suspected breakup events are believed to take place in and near GEO (see also [8-10]). Their origin objects are upper stages except for OI#10365 and OI#11561 (Ekran spacecraft), and their event

dates are between 70's and 90's. All suspected events are assumed to be true and fragments from each event are generated using the NASA standard breakup model. We can confirm whether the suspected events really take place or not by searching fragments from the events based on the present strategy.

Table 1. Suspected breakup events [8-10]

Class (# of objects)	Object identification number (OI#)
Upper stage (23)	2222, 2868, 3292, 3432, 6976, 8751, 11147, 11940, 13089, 14333, 14394, 15630, 16339, 16676, 19347, 19686, 19931, 20926, 21041, 21052, 21762, 21824, 22213
Space craft (2)	10365, 11561

3.2 Simulation Conditions

Table 2 summarizes simulation conditions to process spherical forecasts and **p** distributions. Observations are planned to conduct using the JAXA's observatory at Mt. Nyukasa in Nagano Prefecture, Japan. The observatory has an optical instrument of 35 cm aperture telescope (Takahashi ε-350) and back-illuminated 2k2k CCD sensor (e2v CCD42-40). The observations are decided to conduct during new moon terms in March 2010. As for debris generation, fragments down to 10 cm in size, consist with the current minimum detection size for GEO, are generated. Regarding orbital propagation, snapshots are generated every 5 minutes during 24 hours in the first day of the observation duration. The 24 hours simulation duration considers canceling the uncertainty of estimated breakup position of spacecrafts in an orbit by integrating orbital parameters on GEO period (~ 24 hours). The 24 hours simulation duration is also sufficient to predict population and motion of debris for one-week order observation duration because perturbation effects are small enough to be neglected for one-week orbital propagation.

Table 2. Simulation conditions

Observation site [11]	JAXA's Mt. Nyukasa observatory Longitude: 138° 10' 18"E, Latitude: 35° 54' 05"N, Altitude: 1870 m
CCD dimension [11]	Field-of-View: 1.28° × 1.28°, Resolution: 2.25", Size: 2048 px × 2048 px
Observation duration	2010 March 13th ~ 19th, 20:00 ~ 28:00 JST (one week around new moon)
Size range of generating debris	≥10 cm
Simulation duration	2010 March 13th 0:00 ~ 24:00 JST
Time step to generate snapshots	5 minutes

Subject to the conditions in Tables 1 and 2, debris fragments from 25 breakup events are generated. Fig. 3 indicates that their orbital plane distributions at a snapshot have two major groups. Only the debris fragments from the OI#8751 breakup event distributions far apart from other debris fragments because the OI#8751 breakup event is assumed to have occurred at a high inclination of about 25 degrees that other parent objects would not experience. As will be presented later, this tendency will appear in the spherical forecasts as the completely different distribution

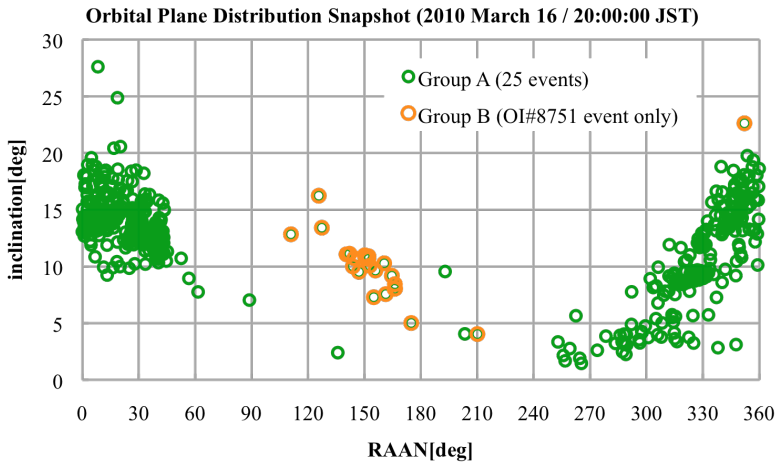

Fig. 3. Orbital plane distribution at a snapshot

between OI#8751 and others. Thus, this paper decided to analyze two different targets; Group A) all breakup events, and Group B) only OI#8751, and specifies two different observation regions for each target.

3.3 Population Prediction & Observation Planning

Subject to the conditions in Table 2, 60 MC runs are carried out to generate spherical forecasts of Group A and Group B as shown in Fig. 4(a) and Fig. 4(b), respectively. The probability density in Fig. 4 is normalized in such a way that the sum of individual probability density becomes one. Brighter regions indicate that debris fragments may exist at a higher density. Each forecast explains the presence density of debris by stacking all orbits propagated, and most overlapped regions indicate that the debris fragments may exist at a highest frequency. The presence probability density at the brightest bin in each forecast is 20~30 times higher than the averaged probability density. From Fig. 4(b), debris fragments from a single breakup event form a sine-wave distribution in a spherical forecast because the debris fragments from a single breakup event may be put into orbits similar to the orbit that the event took place [12].

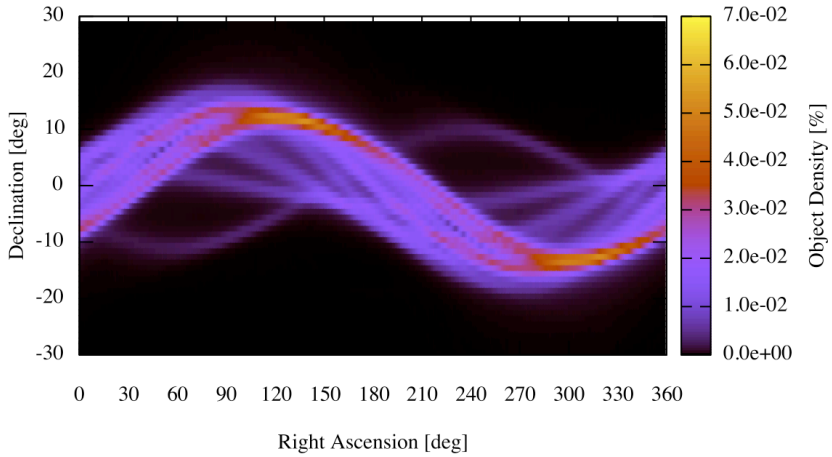

(a) Group A, 60 MC runs, Bin: 1 °×1 °

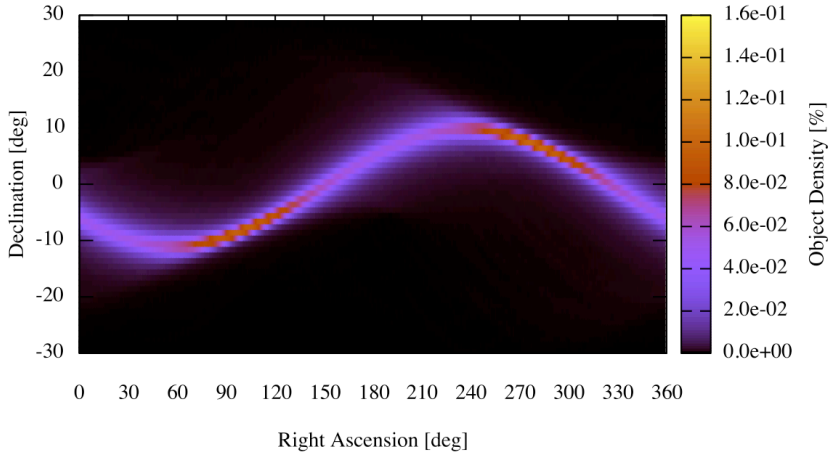

(b) Group B, 60 MC runs, Bin: 1 °×1 °

Fig. 4. Spherical forecasts of group A and B

Observation planning is conducted using the spherical forecasts demonstrated in Fig. 4. As the tracking method of telescope to observe as many debris as possible, we track a fixed RA-Dec coordinate that indicates a higher probability in the forecasts. This paper selects those coordinates as specified in Table. 3. The tracking ranges from

the site are set to fine-tune tracking speed for GEO region. The 8 hours observation duration per day is spared to region A for first 4 hours, and region B for next 4 hours. Table 3 also specifies observation sequences to acquire spatial-temporal images. While acquiring a set of spatial-temporal images, a telescope stops RA-Dec tracking to be fixed to the sky (azimuth-elevation). Sky fixed observation can capture GEO debris in images longer duration than RA-Dec fixed observation because the relative velocity of debris from the site is smaller for the former observation. Imaging conditions to get a set of spatial-temporal images (3 s exp. × 18 shots in 5 minutes) are defined by the constraints such as readout time of CCD and drifting speed of planned RA-Dec region at field-of-view during fixing azimuth-elevation.

Tables 3. Summary of planned observation

(a) Observation region and duration

Group	A	B
Tracking RA-Dec Region (Geocentric)	RA: 120.0 ° Dec: 12.5 ° Range: 42500 km	RA: 240.0 ° Dec: 10.0 ° Range: 43500 km
Duration	20:00 ~ 24:00 JST	24:00 ~ 28:00 JST

(b) Observation sequences

Step1	Stop RA-Dec fixed tracking and fix for azimuth-elevation
Step2	Acquire 1 set of spatial-temporal images (3 s exp. × 18 shots)
Step3	Restart RA-Dec fixed tracking 5 minutes after Step1

3.4 Motion Prediction

Fig. 5 demonstrates the **p** distributions at the targeting regions A and B under conditions specified in Tables 2 and 3. Each **p** distribution represents the presence probability density of **p** that will be appeared in spatial-temporal images at the planned observation regions A and B. The probability density in Fig. 5 is normalized with respect to the summation of binned values in a RA-Dec sphere, so that each **p** distribution counts the presence frequencies of debris fragments on spatial temporal images, and the summation of probability density on each **p** distribution becomes on the order of 0.1 %. The presence probability density of **p** at the brightest region is 10 – 30 times higher than the averaged probability density. Fig. 5(b) indicates that the **p** distribution of fragments from a single breakup event form a clear and unique distribution. Therefore, we may also recognize each **p** distribution in Fig. 5(a) as the outcome of a single breakup event.

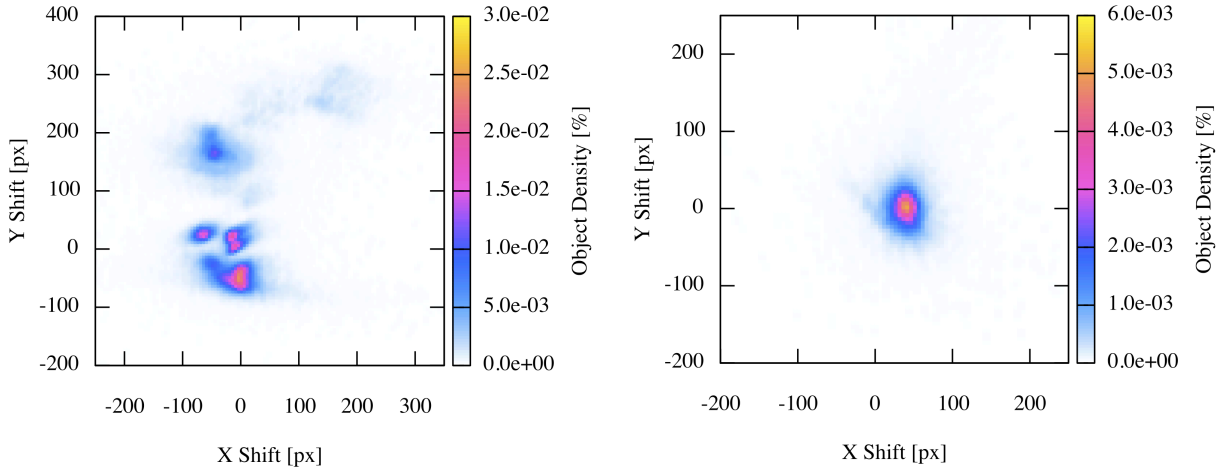

(a) Group A, 100 MC runs, Bin: 5 px×5 px (b) Group B, 100 MC runs, Bin: 5 px×5 px

Fig. 5. **p** distribution of group A and B

Remarking Aspects of p Distribution

Fig. 5 reveals some unique and new aspects on the motion of GEO debris on spatial-temporal images. First, we may be able to identify the origin of detected UCT without further investigation such as backward propagation of its orbit, if the motion vector of UCT appears in a clear, uniform and isolated distribution, especially at a higher probability bin in Fig. 5(a). Once the motion vector of UCT is related to such unique distribution, we may be able to confirm its origin by commonly used backward propagation of both UCT and the parent object of its candidate event.

Fig. 6 compares a possible motion vector region where TBD method needs for superimposing the spatial-temporal images with the actual region of the motion vectors of fragments from a single breakup event. Each image has 2048 by 2048 pixels so that a possible motion vector region quadruples in size as specified in Fig. 6. Yellow-colored region includes all regions where the probability of **p** is higher than 0 % to specify necessary superimposing motion vectors. The area of the yellow-colored region is only 0.38 % of dark region. As demonstrated in Fig. 6, motion prediction can extremely narrow down a superimposing vector area on the order of 0.1 % for each breakup event. This characteristic dramatically helps reducing computational workload that is usually extremely high for computers to analyze images by TBD method.

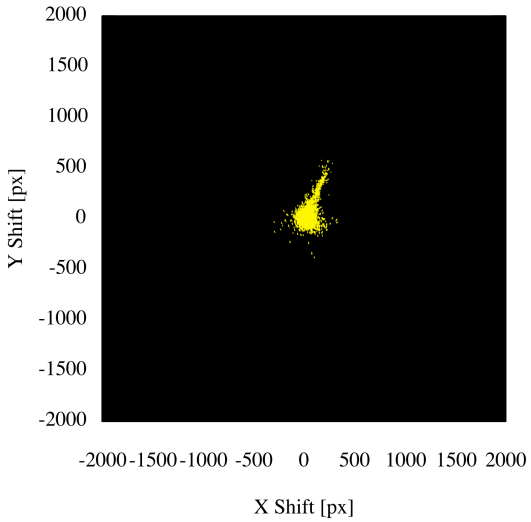

Fig. 6. Extremely narrowdowned superimposing vector area (yellow) by motion prediction (Group B)

Another interesting aspect of motion prediction is that the certain/uncertain **p** distribution regions can be specified by repeating MC runs, especially for the small number of debris fragments from single breakup event that will transit single field-of-view. Here we consider fragments from OI#15630 as an example. Without the Monte Carlo simulation, the motion vectors scatter in **p** distribution and we cannot specify which plot has certainty and which plot has uncertainty (see Fig. 7(a)). With the Monte Carlo simulation, the tendency of **p** distribution appears clearly and uniformly (see Fig. 7(b)) and certain/uncertain **p** regions can be assessed.

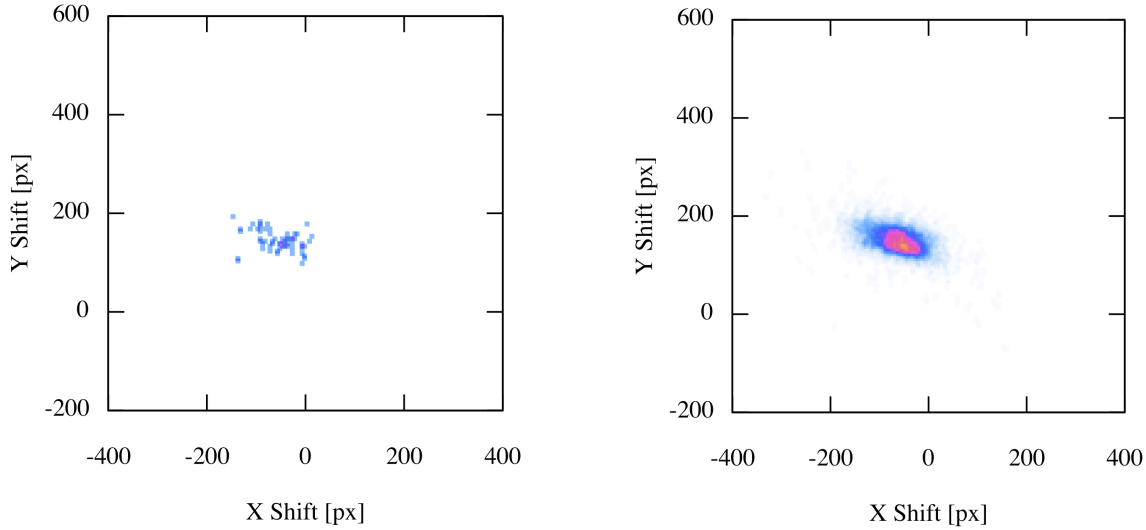

(a) **p** distribution by 1 deterministic run (b) **p** distribution by 100 MC runs

Fig. 7. Monte Carlo simulation specifies the certain / uncertain regions on **p** distribution (OI#15630)

4. COMPARISON WITH MEASUREMENTS

According to the observation plan shown in Tables 3, 5-night observation were carried out and 7614 (423 sets) spatial-temporal images were acquired. To analyze acquired images, the linear-detection method is used as DBT-based method, and the stacking method is used for TBD-based method (that is the only existing TBD method aimed for debris detection), both of which have been developed by Yanagisawa et al. [11][13].

First, spatial-temporal images acquired from the planned observation are analyzed by the linear detection method that can detect objects having relatively high S/N and conduct orbit determination to distinguish between CT and UCT [11]. The linear detection method detects 91 objects in total and 33 individual objects. Fig. 8(a) represents the number of detected CTs and UCTs for each event and each date by the linear detection method. Most of detections belong to region A and only 2 detections belong to region B because few cataloged objects are distributed around region B in terms of orbital plane distribution. Fig. 8(b) shows the relative magnitude of detected CTs and UCTs. 16th magnitude is the limiting magnitude by the observation condition at that time and for the linear detection method.

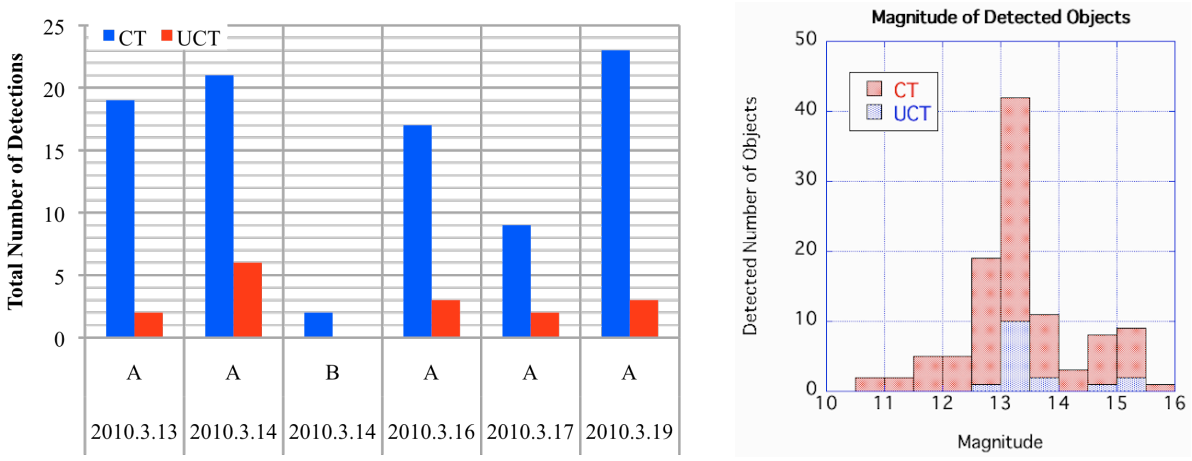

(a) Detection number vs. each date and group (b) Detection number vs. magnitude

Fig. 8. Statistics of detection numbers

Here we compare the distributions of observed motion vectors of UCTs $\mathbf{p}_{UCT}$ detected in region A and calculated $\mathbf{p}$ distribution in region A to verify whether any UCTs have possibility to derive from considered parent objects as discussed in the previous chapter. The result of distribution comparison is shown in Fig. 9. For example, the observed motion vector $\mathbf{p}_{UCT}$ existing near (Δx, Δy) = (-50 px, -20px) belongs to a high probability region formed by

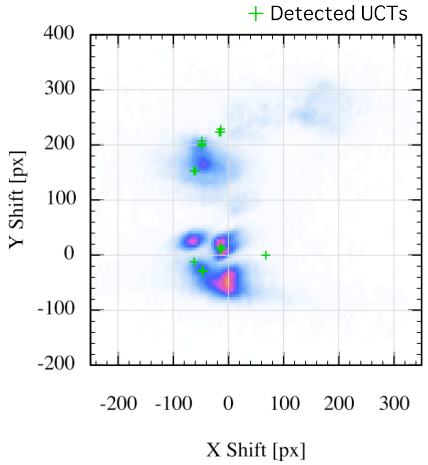

Fig. 9. Verification of $\mathbf{p}_{UCT}$ with $\mathbf{p}$ distribution of region A

OI#20926, and this fact indicates the necessity of further assessments of such UCTs by precise orbital determination of the UCTs and backward propagation of the determined orbit with candidate parent objects.

Next, faint object detections are tried by the stacking method on spatial-temporal images of region B, which have few detection results by the linear detection method. In current version of the stacking method, a region of superimposing vectors has to be defined by a rectangle in **p** distribution. Thus, this paper simply defines a superimposing region in **p** distribution as $\mu \pm \sigma$ (mean and standard deviation, respectively) of given probability distribution (a red rectangle in Fig. 10). Spending two months to analyzing 188 sets of 76023F spatial-temporal images obtained at Region B using a PC (Intel® Core2Duo E6750 2.67GHz, 3.25GB RAM), no additional result is given by the stacking method with supposed superimposing region in **p** distribution. Two reasons of no additional detections are considered as followings:

1. Exposure time and stacking number of images are not sufficient to detect faint debris in spatial-temporal images at least gaining S/N > 1 in a frame
2. The suspected breakup event did not occur in GEO region (OI#8751 explosion breakup event in this case)

The first reason indicates that the probable motion of debris has to be considered at observation planning. The suitable exposure time and stacking number of images should be varied by the debris orbit and characteristic size that we want to detect. If the problem by the first reason is solved and we cannot detect any target faint debris yet, we can conclude that the suspected breakup event did not occur in the history.

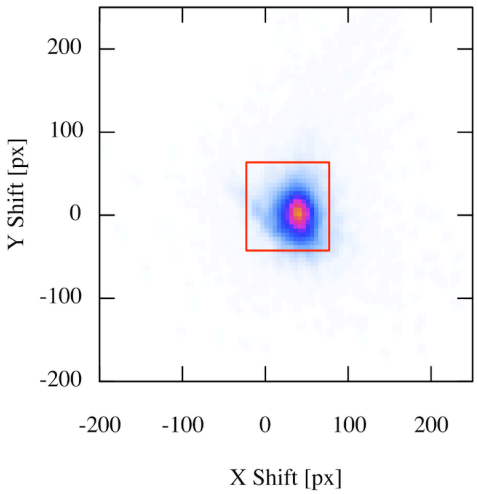

Fig. 10. Superimposing region (red rectangle) on **p** distribution of region B

5. SUMMARY

Applying the ODM-based strategy proposed in this paper, which describes debris generation and propagation to define debris environment, to observation planning and image processing is a unique and innovative way to contribute SSA in GEO. ODM techniques enable us to conduct predictive analyses of space objects that include characterizing, tracking and predicting the behavior of individual and groups of space objects. The predictive analyses specify effectively when, where and how we should conduct optical measurements using ground-based telescopes. ODM techniques also enable us to conduct image-processing methods to effectively decrease limitation on remote imaging of space objects.

The authors have forward-looking research and continuity plan that will mainly focus on the following two topics. First, the proposed ODM-based strategies are to be validated with known breakup event observation such as Titan 3C event in 1992. Second, origin identification procedures are to be developed for the proposed ODM-based strategy. The expanded strategies with origin identification procedures can feed back the information of breakup events confirmed in the planned observation to the supposed breakup events, whether the supposed events have occurred certainly or not.

ACKNOWLEDGEMENTS

The authors would like to give appreciations to Dr. Koki Fujita, Dr. Hiroshi Hirayama, and Mr. Michael Shoemaker of Kyushu University for their useful and practical comments on this study.

REFERENCES

1. Space Track Website, http://www.space-track.org/, United States Strategic Command, Last access confirmed: 2010 June 9th.
2. Schleildknecht, T., et al., "First GEO Survey Test Observations with the ESA 1 m Telescope in Tenerife," Proceedings of the 2000 Space Control Conference, 73-79, 2000.
3. Choc, R. and Jehn, R., "Classification of Geosynchronous Objects," European Space Operations Centre, European Space Agency, Issue 12, 2010.
4. Shoemaker, M.A. and Shroyer, L.E., "Historical Trends in Ground-Based Optical Space Surveillance System Design," Proceedings of the Advanced Maui Optical and Space Surveillance Technologies Conference, Maui, Hawaii, p.E1, 2007.
5. Schildknecht, T., "Optical Surveys for Space Debris," The Astronomy and Astrophysics Review, Vol.14, Issue 1, 41-111, 2007.
6. Gural, P.S., et al., "Matched Filter Processing for Asteroid Detection," The Astronomical Journal, 1951-1960, 2005.
7. Johnson, N.L., et al., "NASA's New Breakup Model of Evolve 4.0," Advances in Space Research, Vol. 28, Issue 9, 1377-1384, 2001.
8. Rykhlova, L.V., et al., "Explosions on the Geostationary Orbit," Advances in Space Research, Vol.19, Issue 2, 313-319, 1996.
9. Johnson, N.L., "Evidence for Historical Satellite Fragmentations in and Near the Geosynchronous Regime," Proceedings of the Third European Conference on Space Debris, 355-359, 2001.
10. Sochilina, A.S., et al., "On the Orbital Evolution of Explosion Fragments," Advances in Space Research, Vol.38, 1198-1202, 2004.
11. Yanagisawa, T., et al., "Activities of JAXA's Innovative Technology Center on Space Debris Observation," Advanced Maui Optical and Space Surveillance Technologies Conference, Poster presentations, 2009.
12. Ikeda, H., et al., "Searching for lost fragments in GEO," Acta Astronautica, Vol. 63, Issue 11-12, 1312-1317, 2008.
13. Yanagisawa, T., et al., "The Stacking Method: The Technique to Detect Small Size of GEO Debris and Asteroids," JAXA Research and Development Report, Japan Aerospace Exploration Agency, JAXA-RR-07-032E, 2008.